



Numerical simulation and experimental validation of novel hyperelastic micro-motion manipulator for water conserving device

Yi-Cheng Huang¹ · Huan-Chu Hsu¹

Received: 27 November 2017 / Accepted: 15 December 2017 / Published online: 21 December 2017
© Springer-Verlag GmbH Germany, part of Springer Nature 2017

Abstract

The aim of this study was to evaluate a novel water-conserving micro-motion manipulator (manipulator) for application in the fluid flow rate regulator of a faucet through numerical simulation and experimental validation. The manipulator was analyzed with various diameters of the water channel. When the channel is narrow, the water flow rate decreases, and the water channel becomes narrower as the inlet water pressure increases. Moreover, the water channel returns to the rest position and provides the required minimum flow rate when the inlet water pressure is minimum. The behavior of the manipulator was simulated using the fluid–structure interaction model of COMSOL multiphysics. The Mooney–Rivlin two-parameter model was used for the simulation. This study employed two methods to obtain the coefficients C_{10} and C_{01} . The first method was performed according to Gent’s relation, a relation between the ASTM D2240 Shore hardness and Young’s modulus. The second method was employed to validate the coefficients during the simulation on the basis of tensile tests performed according to ASTM 412-C. Through the simulations and laboratory testing, the manipulator complies with the requirements of the California Energy Commission (CEC) and U.S. Environmental Protection Agency (EPA). The results show that the physical samples of the manipulator installed in the water-conserving regulators complied with the CEC and EPA standards. The experimental validation results confirmed the suitability of the numerical simulation in predicting the water-conserving performance of the manipulator with respect to the inlet water pressure by using a hyperelastic silicone rubber material.

1 Introduction

A warm climate affects the water supply of a region. Due to the severe conditions faced during droughts, some states such as California have established agencies to manage water resources and the effects of droughts. The energy efficiency and water standards of the California Energy Commission (CEC) require water appliances to consume less water in order to lower energy consumption during appliance use. The CEC standards limit the flow rate to 1.2 gallons per minute (GPM) for residential lavatory faucets and 1.8 GPM for kitchen faucets (California Energy Commission 2015a, b). WaterSense, a U.S. Environmental Protection Agency (EPA) program, has specified that the minimum flow rate should be 0.8 GPM when the inlet water pressure is 20 psi (U.S. Environmental Protection

Agency 2007). Some approaches such as designing, modifying, and replacing faucet equipment have been used to conserve water. One water-conserving method is to install a fluid flow aerator in water-supply devices such as faucets and showerheads. An aerator mixes air into the water, and the water is output in multiple thin streams, providing an economical and functional means of conserving water.

Several inventions (Keppel 1974; Marty et al. 1986; Sochtig 2004) related to the design of water-conserving water-supply devices by using elastic ring deformation have been developed. However, such devices are subject to elastic ring failure for various reasons, such as damage due to frequent contact between the rings and sharp edges. Moreover, ring deformation may fail as a result of abrasion against wall surfaces along the designed paths. This paper presents a robust manipulator design that overcomes the problems faced when using elastic ring deformation. Hyperelastic silicone rubber can be used as a water-conserving manipulator because of its high elongation, incompressibility, reversibility, and mechanical strength; the long-term stability of its hardness; and its long service

✉ Yi-Cheng Huang
ychuang@cc.ncue.edu.tw

¹ Department of Mechatronics Engineering, National Changhua University of Education, Changhua 50074, Taiwan

life (Korochkina et al. 2008). The manipulator was designed such that it could be installed in the regulator of a faucet to provide a uniform and splash-free water flow.

The manipulator provides satisfactory water-conservation ability. A flowchart of numerical simulations of and experiments on the water-conserving manipulator installed

in a regulator is presented in Fig. 1. Figure 2a shows a sectional view of the water-conserving regulator design, and Fig. 2b shows an exploded view of the US patented regulator (Wu 2017) examined in this study.

Hyperelastic rubber enables adjusting the diameter of a water channel and thus conserving water. However, the

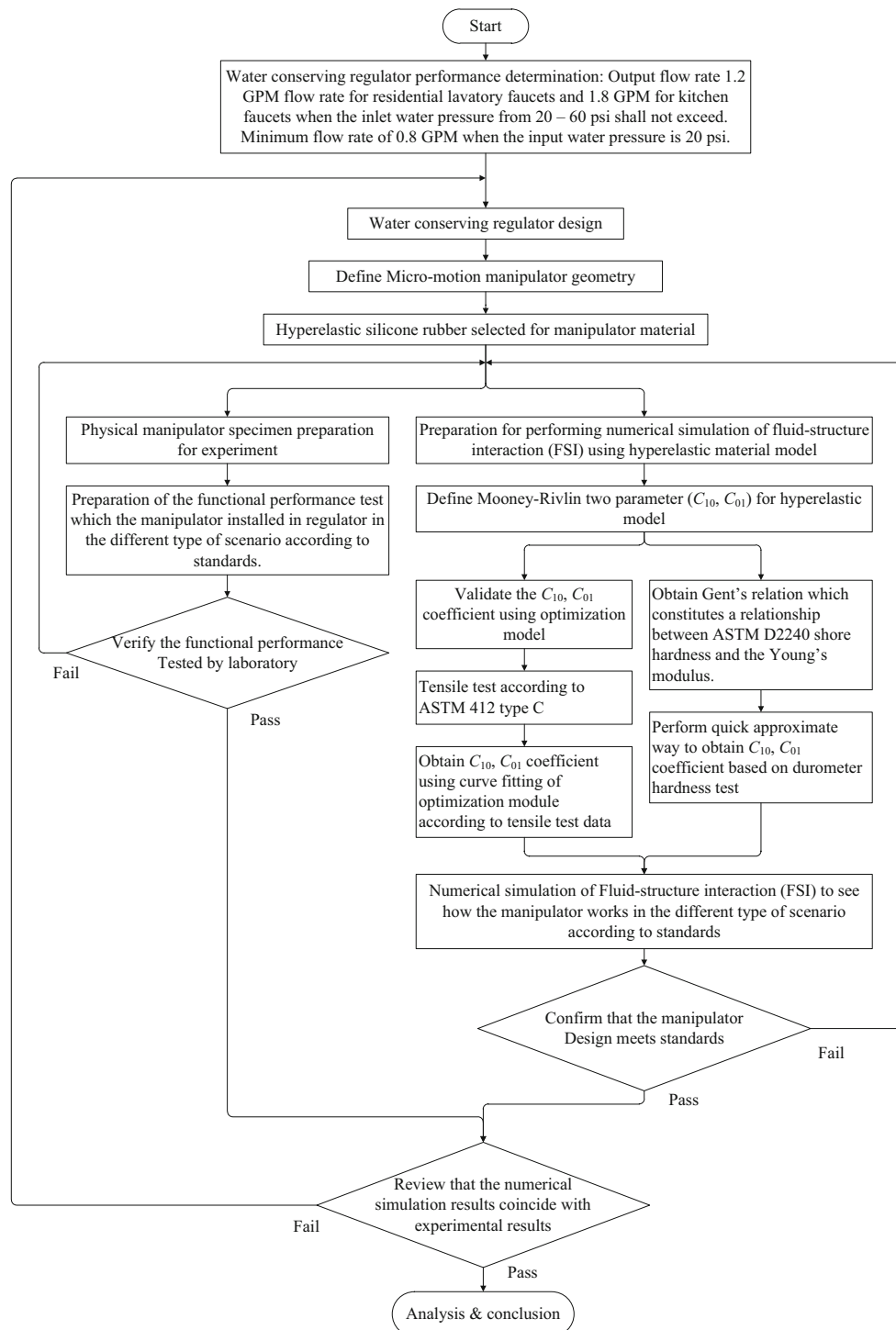
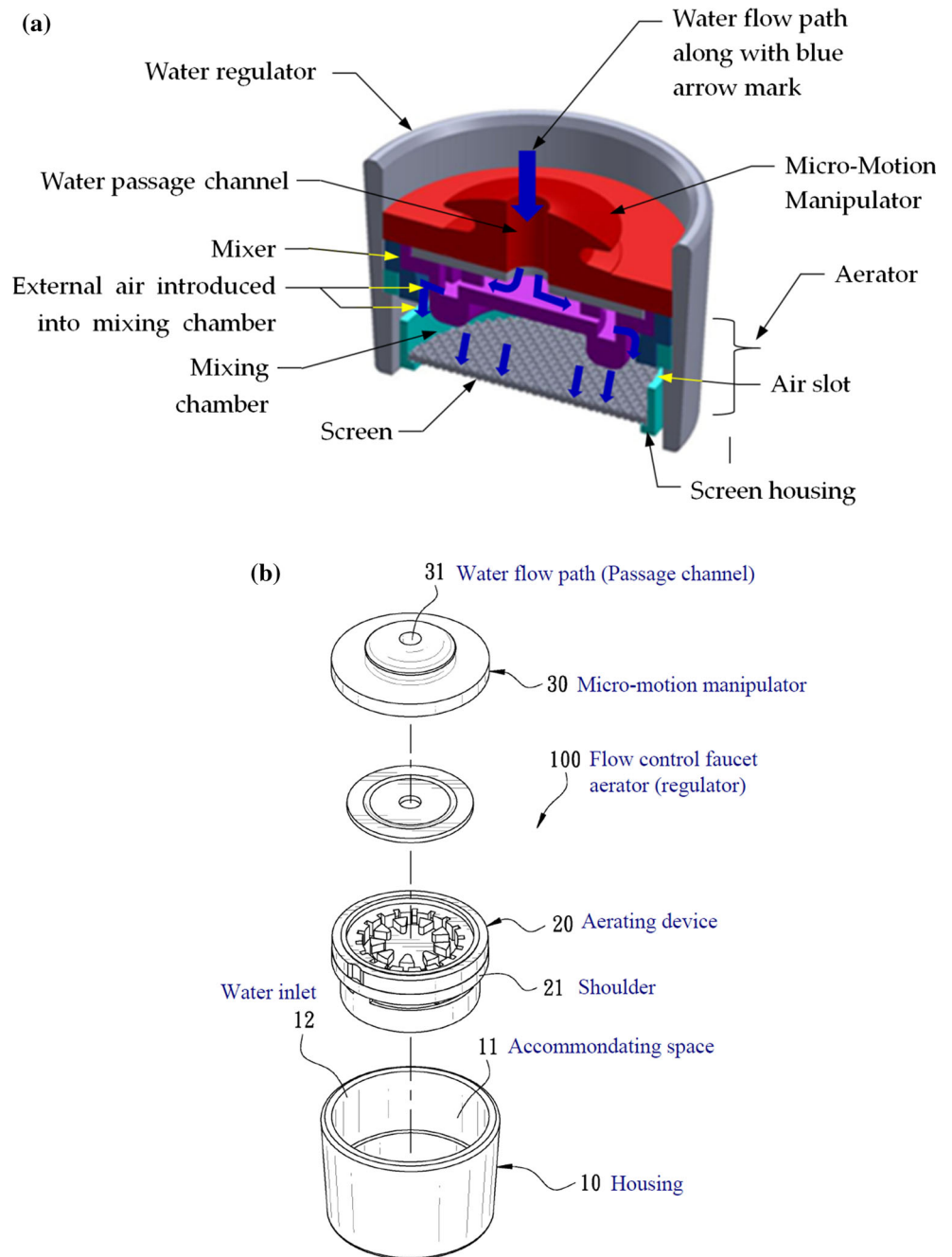


Fig. 1 Flowchart of the numerical simulations of and experiments on the water-conserving regulator

Fig. 2 Illustration for the design of the water flow regulator. **a** Sectional view. **b** Exploded view (Wu 2017)



rubber is a nonlinear material, and selecting a suitable material for the specified inlet water pressure and outlet water flow rate is important. This study used a hyperelastic module to simulate hyperelastic silicone rubber deformation behavior. A suitable material was selected, and the manipulator design was optimized using numerical simulation modeling. The experimental validation results agree with the numerical simulation results.

COMSOL multiphysics software (COMSOL, Inc., Burlington, MA, USA), a finite element analysis tool, was used for the numerical simulations in this study (COMSOL

Inc. 2016a). A numerical simulation of fluid–structure interaction (FSI) was performed using hyperelastic material models. The Mooney–Rivlin two-parameter model was used to define the material properties of the hyperelastic silicon rubber manipulator. Fabricated water-conserving regulator specimens and silicone rubber specimens underwent tensile tests and durometer hardness tests for physical experimental validation. Long Tai Copper Corporation holds patents for the regulators under the Taiwan patent number M512039 and US patent number US2017/0022693 A1 (Wu 2017). This study obtained the coefficients C_{10} and

C_{01} prior to the simulation by using two methods that are explained in Sect. 2.2. A functional simulation of the manipulator was conducted to evaluate coupled nonlinear FSI by using the relevant COMSOL module. The profile and shapes of the manipulator were determined through the numerical simulation results and experiments.

This study verified that the designed manipulator complies with the water-conservation requirement and flow regulations by (1) creating numerical simulation model elements according to evaluation of coupled nonlinear FSI by using the COMSOL module, (2) analyzing the outlet flow rate (GPM) controlled by using the manipulator on the basis of the specified standards of the CEC and Water-Sense, and (3) performing an experimental test in the certified International Association of Plumbing and Mechanical Officials laboratory (IAMPO).

2 Problem formulation

2.1 Methodology

The designed manipulator installed in the regulator for water conservation is shown in Fig. 2a. The blue arrows denote the direction of the water flow. The pressurized inlet water flows into the regulator housing, and the manipulator absorbs force of the inlet water pressure and adjusts the diameter of the major flow channel accordingly. The water output flow rate is dependent on the inlet pressure and the motion of the manipulator. The water then flows into the aerator, which mixes the water and air, thus reducing noise. The outlet water contains a mixture of water and air bubbles, generating soft water flow and thus facilitating water conservation. Figure 2b shows an exploded view of the regulator (Wu 2017).

The properties of the selected silicone rubber material are tabulated in Table 1.

Table 1 Properties of the hyperelastic silicone rubber material of the manipulator

Testing conditions and terms		Result
	Hardness, Shore A (S)	60
Standard testing	Tensile strength (kg/cm ²)	76
Press cure 175 °C/420 s		
Post cure 200 °C/4 HR	Elongation (%)	350
	Specific gravity	1.176

2.2 Theoretical background

The Mooney–Rivlin two-parameter model was used to define the material properties of the hyperelastic silicone rubber manipulator. The coefficients C_{10} and C_{01} for the material model were determined per the simulation requirements by using two methods. In the first method, the coefficients were calculated using an equation on the basis of durometer hardness testing, and the relationship between the Shore hardness and Young's modulus was evaluated using Gent's relation (Brown 1999, 2006; Ucar and Basdogan 2017). The second method involved fitting a curve to tensile test data by using the COMSOL Optimization Module (Korochkina et al. 2008; Li et al. 2012; Azmi et al. 2014). To perform numerical simulations by using hyperelastic rubber models, C_{10} and C_{01} were calculated using both aforementioned methods. The first method is a rapid and simple method for approximately calculating the coefficients C_{10} and C_{01} . By using the first method, the applicable C_{10} and C_{01} coefficients were obtained rapidly, and FSI simulation of the manipulator was successfully performed using COMSOL with hyperelastic material models (COMSOL Inc. 2016b, c, d). The second method was used to verify the coefficients C_{10} and C_{01} for manipulator material selection and simulation validation.

Shore defined and developed a hardness scale and a measurement meter, known as a durometer that are useful for the Shore hardness test of elastomers. Shore hardness provides an indirect measure of the Young's modulus of elastomers. Gent has derived a semiempirical relation between the ASTM D2240 Shore hardness and the Young's modulus of elastomers (Gent 1958; Brown 1999, 2006; Ucar and Basdogan 2017). This relation is as follows:

$$E = \frac{0.0981(56 + 7.62336S)}{0.137505(254 - 2.54S)} \quad (1)$$

where E is the Young's modulus in MPa, and S is the ASTM D2240 Shore hardness. The first method for calculating C_{10} and C_{01} has been empirically developed to obtain the Mooney–Rivlin coefficients. The specified methods are useful because the coefficients are obtained quickly and easily through hardness testing and calculation to experimentally obtained data (Hocheng and Nien 2006; Hirai et al. 2001). The method was conducted as follows.

First, the Shore hardness of the silicone rubber was tested. The value of S was recorded and converted to the Young's modulus, as shown in Eq. (1). The specimens were prepared as shown in Fig. 3.

According to the literature, C_{10} and C_{01} can be derived from the following equations (Hocheng and Nien 2006; Hirai et al. 2001; Charlton et al. 1994):

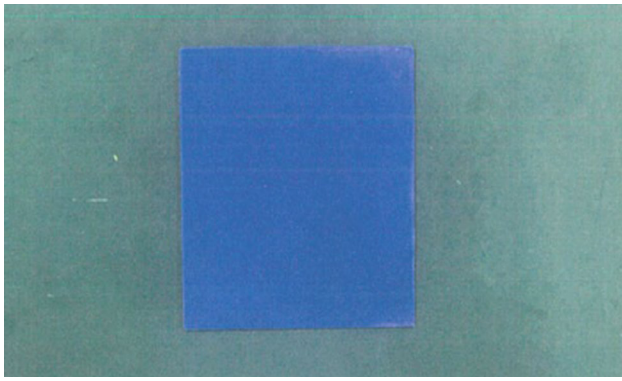


Fig. 3 Picture of the test specimen for ASTM D2240 Shore hardness

$$C_{01} = 0.25 \cdot C_{10} \tag{2}$$

$$6(C_{10} + C_{01}) \approx E \tag{3}$$

The first method was conducted before the numerical simulations. The *S* value of the provided silicone rubber was calculated to be 59.2, and the Young’s modulus was 3.5 MPa. The Mooney–Rivlin C_{01} and C_{10} coefficients were calculated to be approximately 0.5 and 0.1 MPa, respectively. This study performed several numerical FSI simulations for the relationship between the inlet and outlet water flow rate and boundary conditions. The calculated coefficients were $C_{10} = 0.6$ MPa and $C_{01} = 0.1$ MPa, and the simulations were verified to accurately model the functional performance of the manipulator.

By using the second method, curve fitting optimization according to tensile testing data was performed as follows: the specimens were prepared and subjected to uniaxial tensile testing according to ASTM D412-C (Korochkina et al. 2008; Li et al. 2012; Azmi et al. 2014) at the laboratory of the Plastic Industry Development Center, as shown in Fig. 4. The left photo was taken before the tensile test, and the right one was taken after the tensile test. The Mooney–Rivlin two-parameter hyperelastic material model requires coefficients C_{10} and C_{01} , which are determined through curve fitting to uniaxial tensile testing data by

using COMSOL’s optimization Module according to Eq. (4) (COMSOL Inc. 2016b).

$$P = 2 \left(\lambda - \frac{1}{\lambda^2} \right) \left(C_{10} + \frac{1}{\lambda} C_{01} \right) \tag{4}$$

$$\lambda = 1 + \varepsilon$$

where P denotes the measured values of engineering stress representing the force per unit reference area, ε is the strain, and λ is the relative elongation. The coefficients C_{10} and C_{01} were obtained by performing curve fitting to tensile test data by using COMSOL’s Optimization module, as shown in Fig. 5 (COMSOL Inc. 2016b, c).

Ten specimens were subjected to tensile tests. Curve fitting to the tensile test results is presented only for specimen 1 to provide an example of curve fitting and the format of the plots. Specimens 2–10 behaved similarly; thus, their plots and raw data are not presented in this paper. The data of specimen 1, including the results from the tensile test are tabulated in Table 2 (Azmi et al. 2014). The testing time interval was increased from 0.1 to 0.5 s so that data could be tabulated conveniently; recording tensile test data every second provided a large amount of data. However, the recording interval was 0.1 s for curve fitting to tensile test data by using COMSOL’s optimization Module, as shown in Fig. 5. The figure shows that the values of the coefficients C_{10} and C_{01} were 0.7 and 0.1 MPa, respectively, when curve fitting to the tensile test data was performed using COMSOL’s optimization module. This confirms that the calculated values of C_{10} and C_{01} were suitable for material selection and simulations.

This study used the FSI model of COMSOL multi-physics, which combines a fluid flow with solid mechanics to capture the interaction between the fluid and solid structure. The solid mechanics interface and single-phase flow interface were used to model the silicone rubber manipulator and water, respectively. The FSI couplings appear on the boundaries between the water and rubber. The FSI interface uses an arbitrary Lagrangian–Eulerian method to combine a fluid flow formulated using an Eulerian description and a spatial frame with solid



Fig. 4 ASTM D412-C tensile test specimens

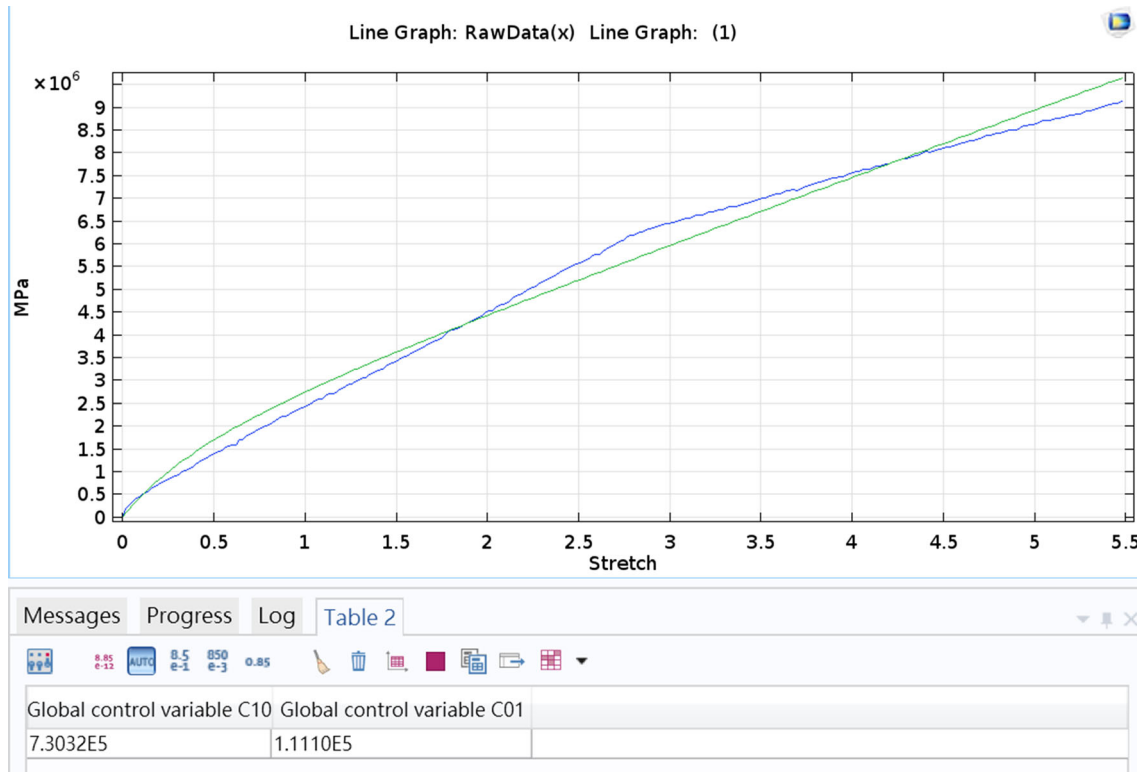


Fig. 5 Obtained C_{10} and C_{01} coefficients through by COMSOL’s optimization module

Table 2 Tensile test results of specimen 1

Stress (Mpa)	0.00	0.50	1.00	1.50	2.00	2.50	3.00	3.50	4.00	4.50	5.00
Stretch	1.00	1.11	1.32	1.55	1.78	2.03	2.28	2.53	2.77	2.99	3.22
Stress (Mpa)	5.50	6.00	6.50	7.00	7.50	8.00	8.50	9.00	9.16		
Stretch	3.46	3.71	4.03	4.50	4.96	5.38	5.85	6.36	6.49		

mechanics formulated using a Lagrangian description and material frame (COMSOL Inc. 2016a, c; Reuter et al. 2017).

The fluid flow in the channel is described using the incompressible Navier–Stokes equations for the velocity field $u_{fluid} = (u, v)$ and the pressure p in a spatial (deformed) moving coordinate system, as shown in Eq. (5).

$$\rho(u_{fluid} \cdot \nabla)u_{fluid} = \nabla \cdot [-pI + \mu(\nabla u_{fluid} + (\nabla u_{fluid})^T)] + F \tag{5}$$

where I denotes the unit diagonal matrix, and F is the volume force affecting the fluid. Assume that no gravitation or other volume forces affect the fluid; thus, $F = 0$.

$$\rho \nabla \cdot u_{fluid} = 0 \tag{6}$$

Hyperelastic material models in COMSOL were employed. As shown in Eqs. (7)–(12), an isotropic hyperelastic material is defined using its elastic-strain energy density W_s , which is often referred as the energy density and is a function of the elastic strain state. The hyperelastic

formulation provides a nonlinear relation between stress and strain. In COMSOL, the right Cauchy–Green deformation tensor C is used to describe the current state of the strain, and the strain energy density is expressed as W_s . The elastic-strain energy density for the Mooney–Rivlin two-parameter hyperelastic material model is given in terms of two isochoric invariants of the elastic right Cauchy–Green deformation tensors $\bar{I}_1(C_{el})$ and $\bar{I}_2(C_{el})$, and the elastic volume ratio J_{el} (COMSOL Inc. 2016a, c; Reuter et al. 2017).

The Piola–Kirchhoff stress is denoted as S , ∇u_{solid} is the displacement gradient, F is the deformation gradient, v is the left stretch tensor, σ is the Cauchy stress, J_{el} is the elastic deformation gradient, J is the volume ratio, $\det(F)$ is a determinant of the deformation gradient, and \bar{I}_1 and \bar{I}_2 are the scalar invariants of the right Cauchy–Green deformation tensor (COMSOL Inc. 2016a, c; Reuter et al. 2017).

The following hyperelastic material models in COMSOL multiphysics were employed.

Fig. 6 Geometry for the simulation of the hyperelastic rubber manipulator with water using the FSI model

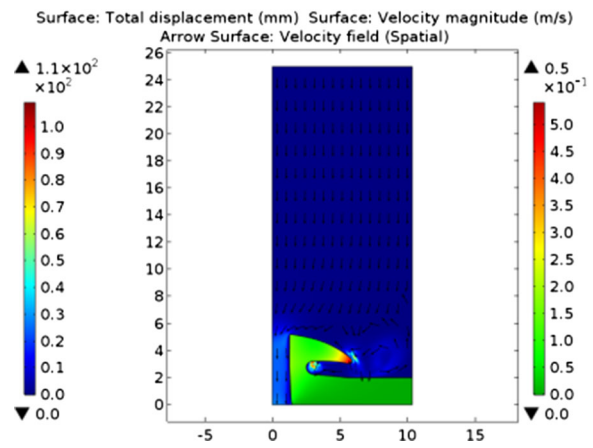
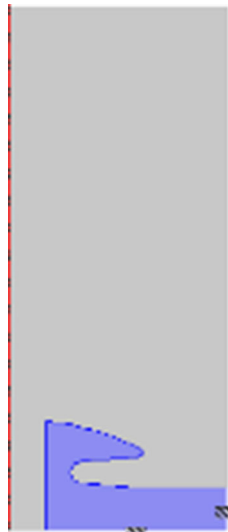


Fig. 9 Water flow field of the manipulator near the channel with an inner diameter of 2.9 mm by an inlet water pressure of 60 psi

Fig. 7 Axisymmetric cross section of the manipulator with water in the regulator housing

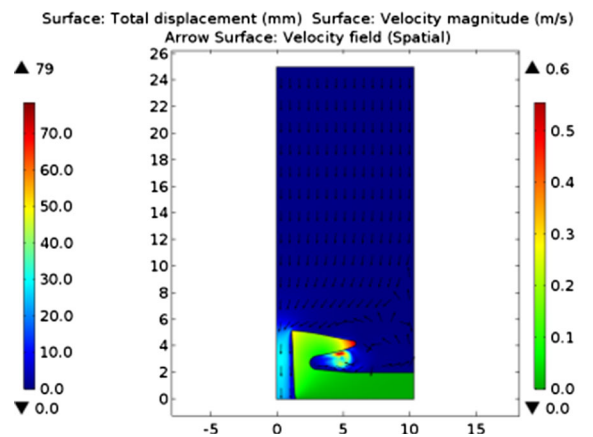


Fig. 10 Water flow field of the manipulator channel with an inner diameter of 2.9 mm by an inlet water pressure of 42 psi

Fig. 8 Mesh plot of the water and micro-motion manipulator

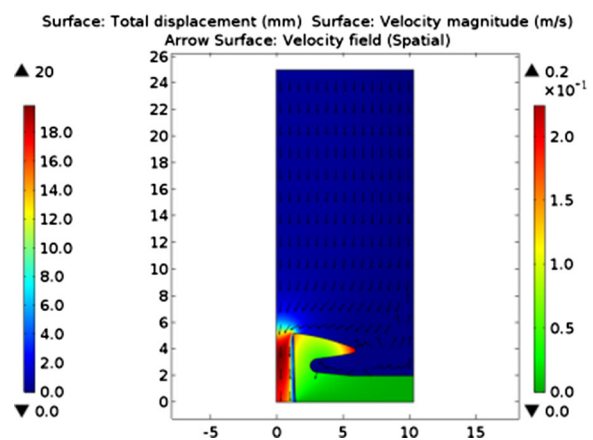
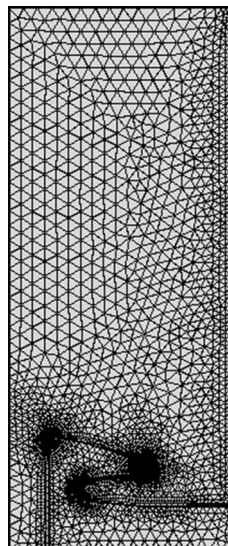


Fig. 11 Water flow field of the manipulator channel with an inner diameter of 2.9 mm by an inlet water pressure of 20 psi

$$-\nabla \cdot \sigma = Fv \quad (7)$$

$$\sigma = J^{-1}FSF^T \quad (8)$$

$$F = (I + \nabla u_{solid}) \quad (9)$$

$$J = \det(F) \quad (10)$$

$$S = \frac{\partial W_s}{\partial \varepsilon} \quad (11)$$

$$W_s = C_{10}(\bar{I}_1 - 3) + C_{01}(\bar{I}_2 - 3) + \frac{1}{2}\kappa(J_{el} - 1)^2 \quad (12)$$

3 Results and discussion

This study performed numerical simulations of the manipulator's functional performance by using the FSI model. The aim was to evaluate the water-conservation performance when the inlet pressure is 60 psi (water flow rate should be less than 1.2 GPM for residential lavatory faucets and 1.8 GPM for kitchen faucets) and 20 psi (water flow rate should be higher than 0.8 GPM). Manipulators with water channels 2.9 and 3.6 mm in inner diameter were evaluated in this study. The functional performance behaviors of manipulators with these diameters were similar. Thus, one of the two diameters was selected as a representative to characterize the performance in different scenarios.

3.1 Numerical simulation results

Figure 6 shows the cross-sectional geometry of the manipulator in an axisymmetric dimension. The blue region is the manipulator, and the gray region is water. Parameters such as the fluid properties, free displacement, boundary wall, axial symmetry, hyperelastic material, inlet

water pressure, outlet flow rate, and boundary constraints were set to complete mesh preprocessing, and computation was then performed. Figure 7 shows the fixed boundary constraint condition of the manipulator in the regulator housing. The blue line denotes the boundary. Figure 8 shows a mesh plot of the water and manipulator.

Figures 9, 10 and 11 show the water flow field of the manipulator near the channel with an inner diameter of 2.9 mm when the inlet water pressure is 60, 42, and 20 psi, respectively. The two coefficients C_{10} and C_{01} of the Mooney–Rivlin model were set as 0.6 and 0.1 MPa, respectively, in the simulation. The color legend on the left in Figs. 9, 10 and 11 denotes the velocity field and that on the right denotes the displacement of the manipulator. The shape of the hyperelastic rubber manipulator changes at different inlet pressures; specifically, the mushroom-like surface of the manipulator bends with increasing inlet pressure. A vortex flow accompanies the hyperelastic rubber manipulator and envelopes its surface. A small vortex with a low pressure preserves the dynamic interaction force between the rubber frame and water fluid field. These observations regarding the mechanism through which the manipulator outputs water demonstrate its function in water conservation.

Figure 12 shows the water flow field of the manipulator with a large channel diameter of 3.6 mm at an inlet water pressure of 60 psi. In the 2D plot (the left plot Fig. 12a) and 3D plot (the right plot Fig. 12b) of the figure, the color legend on the left displays the velocity field and that on the right displays the von Mises stress of the manipulator. The two coefficients C_{10} and C_{01} of the Mooney–Rivlin model had values of 0.6 and 0.1 MPa, respectively. At 60 psi, marked barrel deformation occurs around the middle of the rubber manipulator, conserving water relative to the water output at low pressure. Figure 13 shows the simulation results regarding the deformation of the silicone rubber.

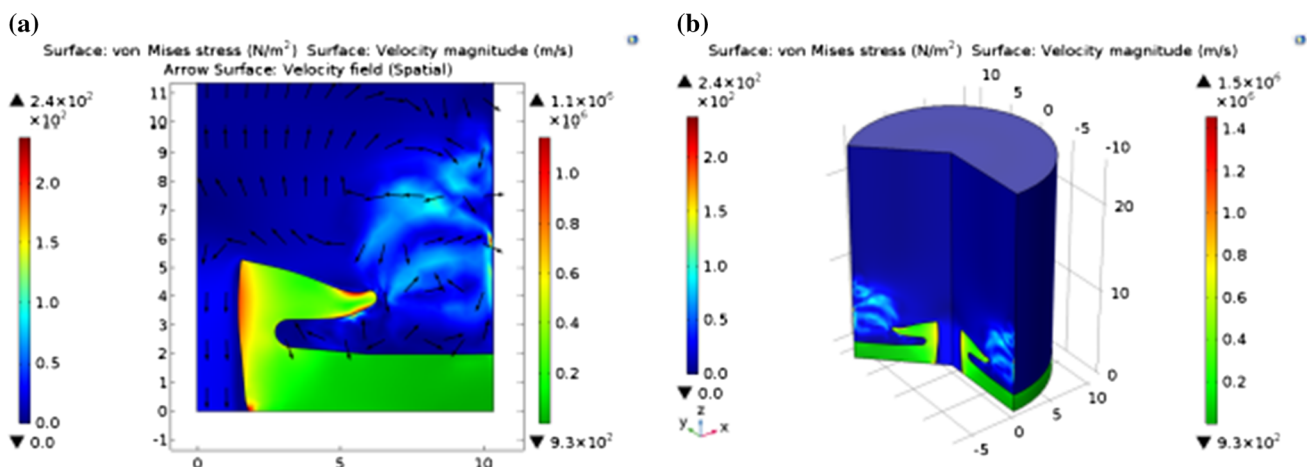


Fig. 12 Water flow field of the manipulator channel with an inner diameter of 3.6 mm by an inlet water pressure of 60 psi

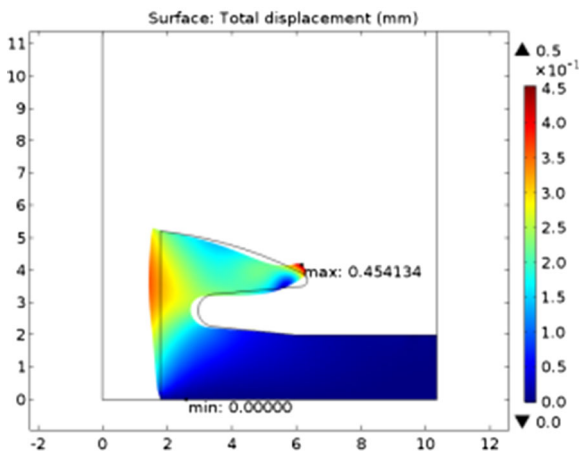


Fig. 13 Maximum displacement plot showing that the inner diameter with inward transverse deformation shape in the middle channel is reduced by 0.71 mm in Fig. 12

The color legend shows the displacement, and the maximum displacement plot shows that the inner diameter of the manipulator decreases by 0.71 mm. This demonstrates that the mushroom-like silicone rubber of the manipulator

shrinks the outflow channel. Thus, water conservation is effectively achieved.

Table 3 shows the output flow rate of the regulator for various diameters of the manipulator channel in the range of 2.6–3.6 mm. The inlet pressure was varied in the range of 20–60 psi with an outlet pressure of 1 atm (normal atmosphere pressure). The numerical simulation results show that the output flow rate is less than 1.8 GPM when the inlet pressure is 60 psi; however, the output flow rate is higher than 0.8 GPM when the inlet pressure is 20 psi. The simulation results comply with the CEC and WaterSense standards for kitchen faucets. The developed hyperelastic rubber manipulator can regulate the water output flow rate with a minimum of 0.8 GPM at a 20-psi inlet water pressure to maximums of 1.2 and 1.8 GPM for lavatory and kitchen faucets, respectively. The correlations between the different inner diameters ranging from 2.9 to 3.6 mm and the associated inlet pressure force are illustrated in Fig. 14. Some curves are not linear because the hyperelastic rubber manipulator heuristically exhibits nonlinear behavior.

Table 3 Numerical simulation results for the output flow rate of kitchen faucets with various inner diameters of the manipulator, outlet flow rate unit: GPM, Mooney–Rivlin coefficients were $C_{10} = 0.6$ MPa and $C_{01} = 0.1$ MPa

		Inlet water pressure				
		20 psi	30 psi	40 psi	50 psi	60 psi
Outlet flow rate						
Inner diameter						
Inner diameters of water passage channel	2.6 mm	0.695	0.757	0.795	0.811	0.871
	2.7 mm	0.785	0.796	0.796	0.828	0.899
	2.8 mm	0.813	0.825	0.884	0.912	0.925
	2.9 mm	0.850	0.919	0.927	0.943	1.010
	3.0 mm	0.920	0.939	0.945	1.077	1.193
	3.1 mm	1.038	1.065	1.102	1.134	1.277
	3.2 mm	1.042	1.087	1.113	1.219	1.289
	3.3 mm	1.076	1.055	1.144	1.254	1.293
	3.4 mm	1.116	1.128	1.211	1.413	1.476
	3.5 mm	1.176	1.197	1.259	1.557	1.614
3.6 mm	1.186	1.235	1.401	1.619	1.635	

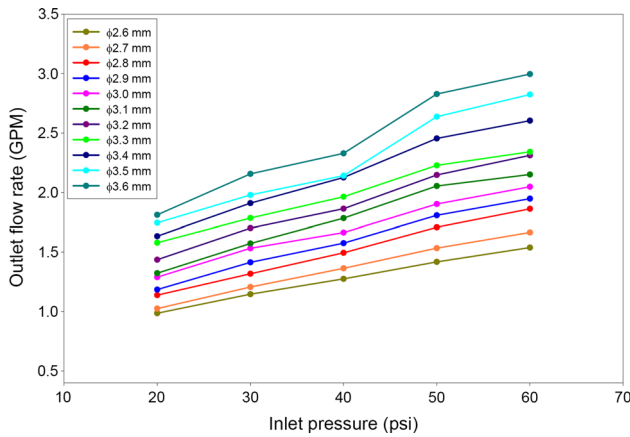


Fig. 14 Profiles of the output flow rate of the regulator with various inner diameters of the manipulator

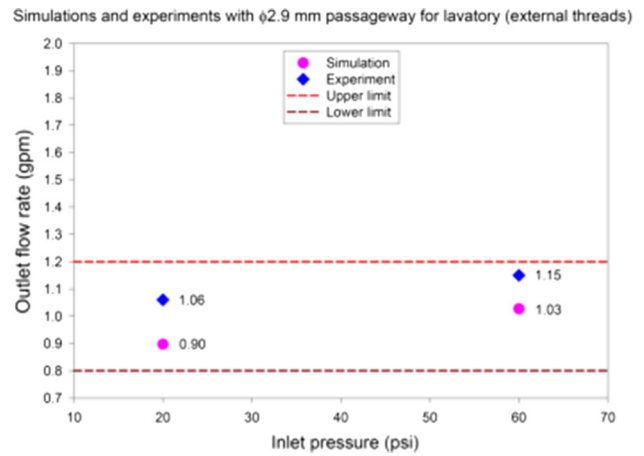


Fig. 17 Plot of the comparison results of numerical simulations and experiments for a 2.9-mm-diameter manipulator channel used in a lavatory

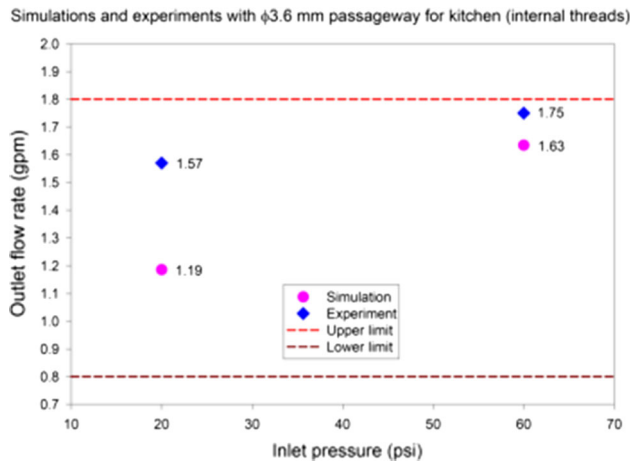


Fig. 15 Plot of the results from numerical simulations and experiments for a 3.6-mm-diameter manipulator channel for use in a kitchen

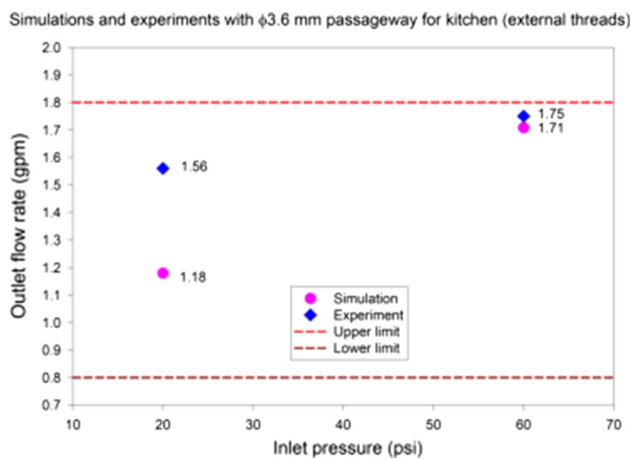


Fig. 16 Plot of the comparison results of numerical simulations and experiments for a 3.6-mm-diameter manipulator channel used in a kitchen

3.2 Experimental results

Figures 15, 16 and 17 show plots of the results from numerical simulation and experimental validation performed by the Metal Industries Research and Development Centre. The numerical and experimental results are within the lower and upper limits when the inlet water pressure is 20 and 60 psi. The numerical simulations and experiments results comply with the CEC Standards for Plumbing Fittings (Table H-3, 2015 appliance efficiency regulations) (California Energy Commission 2015). This study shows that the mathematical model formulated on the basis of nonlinear dynamics solutions in COMSOL simulations yields estimates consistent with the experimental results.

4 Conclusions

A novel water-conserving hyperelastic silicone rubber manipulator was successfully designed and used in a faucet fluid flow rate regulator. The hyperelastic silicone rubber manipulator for controlling the water flow rate was validated using numerical simulation and experimental results. Through academia–industry collaboration, the manipulator was designed in a mushroom-like shape to achieve optimal performance. A high water pressure causes rubber deformation that reduces the diameter of the channel of the manipulator, thus effectively conserving water. At a low pressure, the rubber manipulator returns to its rest position such that the water flow is maintained at or above the specified lower limit of the flow rate. The water conservation function of the hyperelastic silicone rubber manipulator was successfully simulated using the Mooney–Rivlin two-parameter model. The two coefficients C_{10} and C_{01} of this model with hyperelastic nonlinear material were

obtained through two methods. The functional performance of the manipulator was validated using laboratory experiments. The silicone rubber material used for the manipulator has exceptional physical and chemical properties. The material is nontoxic with no environmental pollution, thus complying with the ecological protection requirements and ASME, CSA, NSF, and RoHS standards. This rubber manipulator provides a cost-effective means of conserving water. Moreover, the water flow rate can be effectively controlled to be within the CEC and WaterSense standards by using the regulator.

Funding Funding was provided by Ministry of Science and Technology, ROC (MOST-105-2812-8-018-001).

References

- Azmi NN et al (2014) Testing standards assessment for silicone rubber. In: IEEE International symposium on technology management and emerging technologies
- Brown R (1999) Handbook of polymer testing. CRC Press, New York
- Brown R (2006) Physical testing of rubber. Springer US, New York
- California Energy Commission (2015a) The California Energy Commission, energy commission approves water appliance standards to save more than 100 billion gallons per year. http://www.energy.ca.gov/releases/2015_releases/2015-04-08_water_appliance_standards_nr.html. Accessed 9 Sept 2016
- California Energy Commission (2015b) 2015 appliance efficiency regulations, Table H-3: standards for plumbing fittings, 2015 appliance efficiency regulations. <http://www.energy.ca.gov/2015publications/CEC-400-2015-021/CEC-400-2015-021.pdf>. Accessed 9 Sept 2016
- Charlton DJ et al (1994) A review of methods to characterize rubber elastic behavior for use in finite element analysis. *Rubber Chem Technol* 67:481–503
- COMSOL Inc. (2016a) COMSOL multiphysics 5.2a. Software licensed by COMSOL Inc. Pitotech, Changhua
- COMSOL Inc. (2016b) Fluid–structure interaction, COMSOL multiphysics 5.2a; Theory for the fluid–structure interaction interface, application gallery. <https://www.comsol.com/model/fluid-structure-interaction-361>. Accessed 30 July 2016
- COMSOL Inc. (2016c) Introduction to optimization module, Optimization Module Functionality; Tutorial Example—Curve Fitting. COMSOL multiphysics 5.2a, pp 15–27
- COMSOL Inc. (2016d) Structural Mechanics Module, User’s Guide, Structural Mechanics Theory; Solid Mechanics. COMSOL multiphysics 5.2a, pp 179–512
- Marty Garry R et al (1986) Pressure responsive aerator. US Patent 4,562,960
- Gent AN (1958) On the relation between indentation hardness and Young’s modulus. *Rubber Chem Technol* 31:896–906
- Hirai Y et al (2001) Study of the resist deformation in nanoimprint lithography. *J Vacum Sci Technol B* 19:2811–28152001
- Hocheng H, Nien CC (2006) Numerical analysis of effects of mold features and contact friction on cavity filling in the nanoimprinting process. *J Microlithogr Microfabr Microsyst* 5(1):011004
- Keppel W-D (1974) Fluid flow regulators. US Patent 3,847,178
- Korochkina TV et al (2008) Experimental and numerical investigation into nonlinear deformation of silicone rubber pads during ink transfer process. *Polym Test* 27:778–791
- Li J et al (2012) Hyperelastic property measurements of heat-cured silicone adhesives by cyclic uniaxial tensile test. *J Electron Mater* 41(9):2613–2620
- Reuter T et al (2017) A elastic and hyperelastic material model of joint cartilage—calculation of the pressure dependent modulus of elasticity by comparison with experiments and simulations. https://www.comsol.nl/paper/download/83365/reuter_paper.pdf. Accessed 10 Jan 2017
- Sochtig M (2004) Flow regulator. US Patent 6,695,011
- Ucar H, Basdogan I (2017) Dynamic characterization and modeling of rubber shock absorbers: a comprehensive case study. *J Low Freq Noise Vib Active Control* 1–10
- U.S. Environmental Protection Agency (2007) WaterSense® high-efficiency lavatory faucet specification supporting statement. https://www3.epa.gov/watersense/docs/faucet_suppstat_final508.pdf. Accessed 9 Sept 2016
- Wu F (2017) Flow-control faucet aerator. US Patent US2017/0022693 A1